5

Simulation of Small-pitch High-density Photovoltaic Infrared Focal Plane Arrays

Mikhail Nikitin[1], Albina Drugova[2],
Viacheslav Kholodnov[2] and Galina Chekanova[1]
[1]*Federal State Unitary Enterprise ALPHA*
[2]*Institute of Radio Engineering and Electronics Russian Academy of Sciences*
Russia

1. Introduction

Scanning and starring photovoltaic infrared focal plane arrays (PV IRFPAs) based on ternary alloys $Hg_{1-x}Cd_xTe$ (Whicker, 1992; Triboulet & Chatard, 2000; Baker & Maxey, 2001; Norton, 2002; Kinch, 2007) and binary compound InSb and its alloys (Glozman et al., 2006) are considered as the most sensitive, flexible and perspective for detection of infrared radiation in spectral ranges 1.5-2.7 μm Short-Wave IR (SWIR), 3-5.5 μm Mid-Wave IR (MWIR), 8-14 μm Long-Wave IR (LWIR) and longer than 14 μm Very Long-Wave IR (VLWIR). Those FPAs are updated and improved continuously and move gradually from linear arrays such as 288×4 (TDI); 480×(4-8) (TDI); 768×8 (TDI) pixels to mid-format (sub-TV and TV) including but not limited 64×64; 320×256; 384×288; 640×512 pixels and finally to megapixel format (High Definition TV) like 1280×768; 1280×1024 pixels and more. Nowadays all manufacturers offer LWIR PV FPA with peak wavelength $\lambda_p \approx 8.5\pm0.5$ μm. It means that scanning thermal imagers (TI) based on old LWIR photoconductive (PC) linear arrays ($\lambda_p \approx 11$ μm) covers 8-14 μm atmospheric "window" of transparency totally whereas TI based on LWIR PV FPA with $\lambda_p \approx 8.5\pm0.5$ μm covers left (shorter) part of that "window" only. As the result TIs based on LWIR PC linear arrays ($\lambda_p \approx 11$ μm) allow adequate visualizing of cold landscape (scene) with temperatures as low as minus 60 ^{0}C. Thermal Imagers based on LWIR PV FPA with $\lambda_p \approx 8.5\pm0.5$ μm can visualize adequately cold landscape at scene temperatures higher than minus 30 ^{0}C (even higher than minus 20 ^{0}C). Full replacement of scanning type TI by starring type TI will take place when extended LWIR PV FPA with λ_p shifted to 10-11 μm at T_{op}=80-100 K will become affordable. Megapixel high performance IRFPA having extended spectral covering with λ_p=10-11 μm at T_{op}=80-100 K could be preferable to create future TI systems.

Increasing of array format along with improvement in performance is general development trend in IRFPA technology. It is accompanied inevitably by decreasing of pixel size and pixel pitch to minimal size reasonable from point of view of infrared physics to provide the best resolution and producing comfortable imaging with electro-optic (EO) system. Pitch in small-pitch PV IRFPA can be equal to from 10 μm to 20 μm. PV arrays based on InSb and its alloys or $Hg_{1-x}Cd_xTe$ alloys are fabricated often on single layer (substrate) that is common for all pixels of array.

Implementation of large format high performance PV IRFPAs covering above mentioned spectral ranges both single-color and multi-color requires comprehensive simulation of photodiodes (PD) performance depending on base material layers properties, interfaces parameters, array topology, array design and operating conditions. Analysis of MWIR and LWIR PD performance at operating temperatures from 77 K to 100 K and higher is needed also due to strong tendency to use so called HOT (higher operating temperature) mode for lowering weight and power consumption in perspective TIs with cryogenically cooled megapixel IRFPAs.

Perhaps novel $Hg_{1-x}Cd_xTe$ FPAs will be based on photodiodes with p-n junction opposite to usually used n^+-p junction. PD with optimal p-n junction could have lower dark current value than same size n^+-p junction. It is desirable for adequate multiplexing of PD arrays to Silicon Read-out Integrated Circuits (ROICs).

2. Key aspects of IRFPA performance requiring simulation

1. Simulation of IR photodiodes detectivity and responsivity depending on cut-off wavelength, type of junction: n^+-p junction or p-n junction and operating temperatures from 77 K to 100 K and higher.
2. How does recombination rate at nearest interface to PD absorber impact on PD dark current?
3. Development of theoretical approach producing analytical expressions for collection of photogenerated charge carriers in small-pitch infrared PV arrays enabling optimization of array topology for reaching the best resolution, good filling factor and minimal cross-talking.

Due to small thickness of layers in epitaxial heterostructure interfaces are located close to active regions of p-n junction and hence generation-recombination processes at interfaces can impact on value of current flowing through junction. In high-density arrays with thin common layer, collection length of photogenerated charge carriers will exceed pixel pitch as a rule. It means that each pixel can collect excess charge carriers generated far from PD's p-n junction border. Therefore optimization of resolution, filling factor and cross-talking level of small-pitch high-density PV FPA requires complete estimation of photocurrent generation in neighbor PD pixels depending on pixel and array design, material properties and operating conditions. In two technologically viable 2D IRFPA architectures: front-side illuminated High-Density Vertically Integrated Photodiode (HDVIP) or ("Loop-hole") and backside illuminated flip-chip bonded via In-bumps to Si-ROIC are used special guard rings or grids to solve a. m. problems. Therefore development of theoretical simulation describing analytically collection of photogenerated charge carriers in small-pitch infrared PV arrays seems useful.

3. Simulation of LWIR $Hg_{1-x}Cd_xTe$ PD with small sensitive area

3.1 Photodiode models and simulation approach

Simulation was done for front-side illuminated LWIR $Hg_{1-x}Cd_xTe$ photodiode based on n^+-p or p-n junction. Performance of LWIR photodiodes ($Hg_{0.785}Cd_{0.215}Te$ and $Hg_{0.766}Cd_{0.234}Te$) was estimated at operating temperatures 77 K and 100 K. Evaluation was performed at reverse bias 0.05 V because every real $Hg_{1-x}Cd_xTe$ PD array multiplexed to Silicon Read-out Integrated Circuit (ROIC) is operated under reverse bias.

Upper limit of PD performance was calculated under assumption that diffusion current is prevailing component of dark current in PD pixel at low reverse bias. Photocurrent excited by background radiation was taken into account as well because its value is competitive to dark (diffusion) current. Tunnel current is controlled mainly by total absorber doping and in calculations its value was considered many times lower than diffusion current value at reverse bias 0.05 V. Currents due to generation in space charge region of p-n junction and surface (interface) shunting were ignored. Interface shunting elimination can become the hardest task to solve. Surface (interface) recombination acts as generator of minority charge carriers into absorber region of either n^+-p or p-n junction and at high rates it can enlarge seriously dark current value, especially when p or n absorber region is thin (shorter than diffusion length of minority charge carriers). For simplicity surface recombination rate was taken low (negligible) - 10^2 cm/sec and high (infinitive) - 10^7 cm/sec.

3.2 PD performance: simulation formalism

Let's take photodiode with n-p junction as a model and consider contribution of quasi-neutral n-side and p-side of photodiode to dark current and background current.
Depletion current per unit volume from the n-side for a planar one-side photodiode is given by expression:

$$J_p(-W_n) = J_p^F(-W_n) + J_p^D(-W_n) \tag{1}$$

Density of background current from n-side is described by formula:

$$J_p^F(-W_n) = \eta \times q \times F \times \exp(-\gamma \times W_1) \times \left[\frac{\gamma^2 \times L_p^2}{1 - \gamma^2 \times L_p^2} \right] \times \{1\} \tag{2}$$

$$\{1\} = 1 + \frac{1}{\gamma \times L_p} \times \frac{\frac{D_p}{L_p} \times sh\frac{W_1}{L_p} + S_p \times ch\frac{W_1}{L_p} - (\gamma \times D_p + S_p) \times \exp(\gamma \times W_1)}{\frac{D_p}{L_p} \times ch\frac{W_1}{L_p} + S_p \times sh\frac{W_1}{L_p}} \tag{3}$$

Density of dark current from n-side is described by formulae:

$$J_p^D(-W_n) = -q \times \frac{D_p}{L_p} \times \Delta p_{ne}(-W_n) \times \left[\frac{\frac{D_p}{L_p} \times sh\frac{W_1}{L_p} + S_p \times ch\frac{W_1}{L_p}}{\frac{D_p}{L_p} \times ch\frac{W_1}{L_p} + S_p \times sh\frac{W_1}{L_p}} \right] \tag{4}$$

$$\Delta p_n(-W_n) = p_{ne}\left(\exp\left(\frac{q \times V}{kT} \right) - 1 \right) \tag{5}$$

Contribution to responsivity from n-side of photodiode:

$$S_{J\lambda}^{N} = \eta \times 0.8 \times 10^4 \times \lambda_{co} \times \exp(-\gamma \times W_1) \times \left[\frac{\gamma^2 \times L_p^2}{1 - \gamma^2 \times L_p^2} \right] \times \{1\} \tag{6}$$

$$\lambda_{co}(\mu m) = \frac{h \times c}{E_g(eV)} \tag{7}$$

Depletion current per unit volume from the p-side for a planar one-side photodiode is given by expression:

$$J_n(W_p) = J_n^F(W_p) + J_n^D(W_p) \tag{8}$$

Density of background current from p-side is described by formula:

$$J_n^F(W_p) = \eta \times q \times F \times \exp(-\gamma \times W_1) \times \left[\frac{\gamma^2 \times L_n^2}{(\gamma \times L_n)^2 - 1} \right] \times \{2\} \tag{9}$$

$$\{2\} = 1 - \frac{1}{\gamma \times L_n} \times \frac{S_n \times ch\frac{W_3}{L_n} + \frac{D_n}{L_n} \times sh\frac{W_3}{L_n} + \exp(-\gamma \times W_3) \times [-S_n + \gamma \times D_n]}{S_n \times sh\frac{W_3}{L_n} + \frac{D_n}{L_n} \times ch\frac{W_3}{L_n}} \tag{10}$$

Density of dark current from p-side is described by formulae:

$$J_n^D(W_p) = -q \times \frac{D_n}{L_n} \times \Delta n_{pe}(W_p) \times \frac{\frac{D_n}{L_n} \times sh\left(\frac{W_3}{L_n}\right) + S_n \times ch\left(\frac{W_3}{L_n}\right)}{\frac{D_n}{L_n} \times ch\left(\frac{W_3}{L_n}\right) + S_n \times sh\left(\frac{W_3}{L_n}\right)} \tag{11}$$

$$\Delta n_p(W_p) = n_{pe}\left[\exp\left(\frac{q \times V}{kT} \right) - 1 \right] \tag{12}$$

Contribution to responsivity from p-side of photodiode:

$$S_{J\lambda}^{P} = \eta \times 0.8 \times 10^4 \times \lambda_{co} \times \exp(-\gamma \times W_1) \times \frac{\gamma^2 \times L_n^2}{1 - \gamma^2 \times L_n^2} \times \{2\} \tag{13}$$

Here:

$-W_n$ - coordinate of depletion region border on n-side; W_p - coordinate of depletion region border on p-side; W_1 - thickness of quasi-neutral n-side; W_3 - thickness of quasi-neutral p-side; q - electron charge; $\eta = 1 - r$ - quantum efficiency; γ and r - absorption and reflection coefficients; F - background radiation flux density; D_n, D_p - diffusion coefficient for electrons and holes properly; L_n, L_p - diffusion length for electrons and holes properly; S_n, S_p - surface recombination rate for electrons and holes properly; λ_{co} - cut-off wavelength. Majority and minority charge carrier concentrations are defined (Blakemore, 1962)

In n-side:

$$n = n_e + n_{bgr}\,;\, p_n = p_{ne} + n_{bgr}\,;\; n_e = \frac{N_d}{2} + \frac{\left(N_d^2 + 4n_i^2\right)^{1/2}}{2}\,;\; n_{bgr} = p_{bgr} = g_{bgr} \times \tau_{eff} \tag{14}$$

In p-side:

$$p = p_e + n_{bgr}\,;\, n_p = n_{pe} + n_{bgr}\,;\; p_e = \frac{N_a}{2} + \frac{\left(N_a^2 + 4n_i^2\right)^{1/2}}{2}\,;\; n_{bgr} = p_{bgr} = g_{bgr} \times \tau_{eff} \tag{15}$$

Where:

n_e and p_e - equilibrium electron and hole concentrations; N_d / N_a donor/acceptor dopant concentration; n_i – intrinsic carrier concentration; $n_{bgr} = p_{bgr}$ – average concentration of excess charge carriers generated by infrared background flux; $g_{bgr} = \eta \times \gamma \times F$ – excess charge carriers generation rate by background flux; τ_{eff} - resulting excess charge carriers' lifetime.

Energy gap value $E_g(x,T)$ in eV is determined by formula (Laurenti et al., 1990), where x is composition of $Hg_{1-x}Cd_xTe$:

$$E_g = -0.303 \times (1-x) + 1.606 \times x - 0.132 \times x \times (1-x) + \{3\} \tag{16}$$

$$\{3\} = \frac{\left[6.39 \times (1-x) - 3.25 \times x - 5.92 \times x \times (1-x)\right] \times 10^{-4} \times T^2}{11 \times (1-x) + 78.7 \times x + T} \tag{17}$$

Intrinsic charge carriers concentration in $Hg_{1-x}Cd_xTe$ is given by expression (Schmit, 1970):

$$n_i = 4.293 \times \cdot 10^{14} \times (1.093 - 0.296x + 0.442 \times 10^{-3} \times T) \times T^{3/2} \times E_g^{3/4} \times \exp\left(-\frac{E_g}{2kT}\right) \tag{18}$$

In pure non-compensated $Hg_{1-x}Cd_xTe$ material there are two band-to-band processes which control total recombination rate: radiative recombination and Auger recombination due to transitions A1 and/or A7 (Kinch et al, 1973; Gelmont, 1980; Gelmont 1981; Kinch, 2007):

$$\frac{1}{\tau_R} = \frac{n_e + p_e + n_{bgr}}{2n_i \times \tau_{Ri}}\,;\; \frac{1}{\tau_{A1}} = \frac{(n_e + n_{bgr}) \times (n_e + p_e + n_{bgr})}{2 \times n_i^2 \times \tau_{A1}^i}\,;\; \frac{1}{\tau_{A7}} = \frac{(p_e + n_{bgr}) \times (n_e + p_e + n_{bgr})}{2 \times n_i^2 \times \tau_{A7}^i} \tag{19}$$

$$\tau_{Ri} = 7 \times 10^8 \times (1+\mu)^{3/2} \times \frac{1}{E_g n_i} \times \left(\frac{T}{77}\right)^{3/2}\,;\; \tau_{A1}^i = \frac{1}{7.2 \times 10^{13}} \times \frac{1}{E_g} \times \left(\frac{E_g}{kT}\right)^{3/2} \times \exp\left[(1+2\mu) \times \frac{E_g}{kT}\right];$$

$$\tau_{A7}^i = 3.69 \times 10^{-16} \times \mu^{-5/2} \times \frac{E_g}{kT} \times \exp\left[(1+\mu) \times \frac{E_g}{kT}\right]\,;\; \mu = (m_e / m_{hh})\,. \tag{20}$$

Resulting excess charge carriers' lifetime equals to:

$$\frac{1}{\tau} = \frac{1}{\tau_R} + \frac{1}{\tau_{A1}} + \frac{1}{\tau_{A7}} \tag{21}$$

Iteration procedure was used to calculate n_{bgr} (5): $\tau_{eff}\Big|_{n_{bgr}=n_{bgr}^{(i)}} = \tau_{eff}\Big|_{n_{bgr}=n_{bgr}^{(i-1)}}$, $i = 1, 2, \ldots$ k, $n_{bgr}^{(0)} = 0$. Convergence took place at number of iteration k ≤ 10.

The following noise sources were taken into account:

- Johnson-Nyquist thermal noise of PD's dynamic resistance;
- Background current shot noise;
- Dark current shot noise.

Noise currents densities are taken at preselected reverse bias V_b (typically 0.01-0.1 V).

$$\delta I^2 = \frac{4kT}{R_{dV}}\Delta f + 2 \times q \times (J_{\Sigma}^{Ff} \times A_{Ff} + J_{\Sigma}^{D} \times A_d) \times \Delta f \tag{22}$$

Total density of noise current:

$$I_{sh} = \sqrt{\delta I^2} \tag{23}$$

Here:

A_d - geometrical area of photodiode's p-n junction; A_{Ff} - collection area of photogenerated current in photodiode ("light capture" area); Δf - operative bandwidth; R_{dV} - resistance of photodiode at preselected reverse bias V, J_{Σ}^{Ff} - total background current, J_{Σ}^{D} - total dark current.

$$\frac{1}{R_d} = A_d \times \frac{q^2}{kT} \times \left[-p_n \times \frac{D_p}{L_p} \times \frac{\frac{D_p}{L_p} \times sh\frac{W_1}{L_p} + S_p \times ch\frac{W_1}{L_p}}{\frac{D_p}{L_p} \times ch\frac{W_1}{L_p} + S_p \times sh\frac{W_1}{L_p}} - n_p \times \frac{D_n}{L_n} \times \frac{\frac{D_n}{L_n} \times sh\frac{W_3}{L_n} + S_n \times ch\frac{W_3}{L_n}}{\frac{D_n}{L_n} \times ch\frac{W_3}{L_n} + S_n \times sh\frac{W_3}{L_n}} \right] \tag{24}$$

$$R_{dV} = R_d \times \exp\left(-\frac{q \times V}{kT}\right) \tag{25}$$

First term in curly brackets determinates contribution of n-side to resistance of photodiode at reverse bias and second term the same of p-side.

Impact of surface recombination rate on charge carriers concentration and currents densities was accounted correctly.

Total density of background current:

$$J_{\Sigma}^{Ff} = J_n^{Ff}(-W_n) + J_p^{Ff}(W_p) \tag{26}$$

Total density of dark current:

$$J_{\Sigma}^{D} = J_n^{D}(-W_n) + J_p^{D}(W_p) \tag{27}$$

Let's assume for simplicity that:

$$A_d = A_{Ef} = A \tag{28}$$

Density of total current through photodiode will be sum of two terms:

$$J_{FfD} = J_{\Sigma}^{Ef} + J_{\Sigma}^{D} \tag{29}$$

Detectivity is calculated following to standard expression:

$$D^* = \frac{S_J \times A \times \Delta f}{(\delta I^2)^{1/2}} = \frac{S_J}{\left(\frac{4kT}{R_{dV} \times A} + 2q \times J_{FfD}\right)^{1/2}} \tag{30}$$

$$Ff = k_f \times 2\pi \times c \int_{2\times10^{-4}}^{\lambda_{co}} \frac{1}{\lambda^4} \times \frac{d\lambda}{\exp\left(\frac{h \times c}{\lambda \times kT_{Ff}}\right) - 1} \tag{31}$$

Here: $k_f = \sin^2(\Theta/2)$ where Θ - full solid angle within that background and signal radiation comes in sensitive area of photodiode.

3.3 LWIR PD performance: calculation results

We have done calculations for model photodiodes based on asymmetric n^+-p or p-n junction always used in practice. Data used in calculation are presented in Table 1.

	PD with n^+-p junction		PD with p-n junction	
Operating temperature, T (K)	77	100	77	100
$Hg_{1-x}Cd_xTe$ absorber composition, x (mol. fr.)	0.234 / 0.215	0.234 / 0.215	0.234 / 0.215	0.234 / 0.215
Energy gap, E_g (eV)	0.138 / 0.104	0.144 / 0.112	0.138 / 0.104	0.144 / 0.112
Cut-off wavelength, λ_{co} (μm)	9.0 / 11.9	8.6 / 11.1	9.0 / 11.9	8.6 / 11.1
Peak wavelength, λ_P (μm)	≈ 8.1 / ≈ 10.5	≈ 7.7 / ≈ 10	≈ 8.1 / ≈ 10.5	≈ 7.7 / ≈ 10
Absorption coefficient (Blue, 1964), γ (cm^{-1})	3×10^3	3×10^3	3×10^3	3×10^3
Quantum efficiency, η	0.7	0.7	0.7	0.7
Junction area, A (μm × μm)	20 × 20	20 × 20	20 × 20	20 × 20
Junction regions doping, n and p (cm^{-3})	$n^+=10^{17}$ $p=10^{16}$	$n^+=10^{17}$ $p=10^{16}$	$p=5\times10^{16}$ $n=10^{15}$	$p=5\times10^{16}$ $n=10^{15}$
Junction regions thickness, t (μm)	t(n^+) = 0.5 t(p-absorber) = 4-40	t(n^+) = 0.5 t(p-absorber) = 4-40	t(p) = 0.5 t(n-absorber) = 4-40	t(p) = 0.5 t(n-absorber) = 4-40
Electron mobility, μ_n ($cm^2/(V\times sec)$)	1.9×10^5	1.29×10^5	1.9×10^5	1.29×10^5
Hole mobility, μ_P ($cm^2/(V\times sec)$)	600	390	600	390
Reverse bias value, V_b (V)	-0.05	-0.05	-0.05	-0.05
Surface recombination rate, s (cm/sec)	10^2 10^7	10^2 10^7	10^2 10^7	10^2 10^7

Table 1. Data used for estimation of small-size $Hg_{0.766}Cd_{0.234}Te$ and $Hg_{0.785}Cd_{0.215}Te$ photodiodes performance

Calculation results are presented on Fig. 1-6. Typically discussed photovoltaic case (V_b =0) has been studied as well.

Obtained results presented on Fig. 1-6 say that extended LWIR PD with p-n junction will be potentially of 4-5 times lower dark current value than PD with n+-p junction at T_{op}=77 K and 2 times lower at T_{op}=100 K. As the result it is hoped that decrease in D* value with elevating of operating temperature up to 100 K will be moderate in the case of PD with p-n junction opposite to significant decreasing observed on LWIR PD with n+-p junction as it presented on Fig. 1-6. Calculated detectivity at reverse bias 0.05 V is higher than in the case of zero bias (photovoltaic mode). Formalism of R_0A product is not suitable for the case of LWIR PD arrays multiplexed to Silicon ROIC.

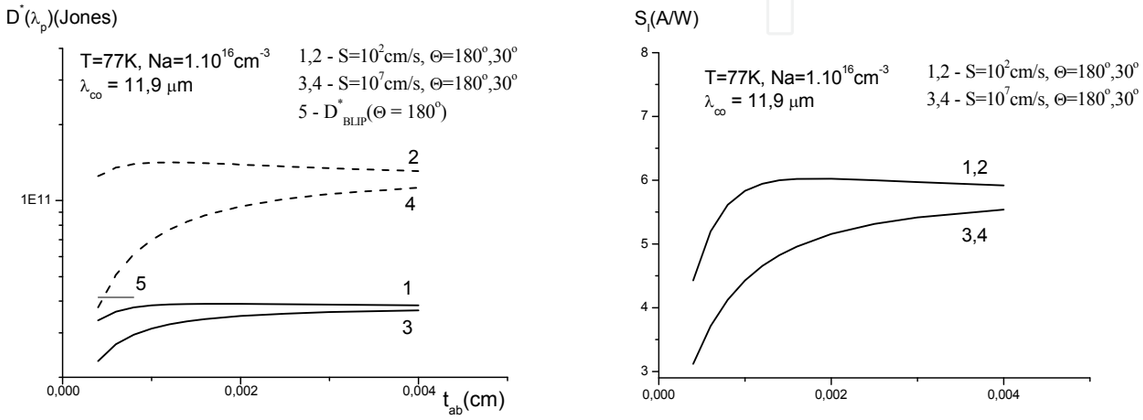

Fig. 1. Calculated peak detectivity $D^*(\lambda_p)$ and peak responsivity $S_I(\lambda_p)$ of $Hg_{0.785}Cd_{0.215}Te$ photodiodes with n^+-p junction versus thickness of p-absorber t_{ab} at FOV=180^0 – (1 and 3) and FOV=30^0 – (2 and 4). Surface recombination rate s=10^2 cm/sec (1 and 2) and s=10^7 cm/sec (3 and 4). Operating temperature 77 K. Background temperature equals to 293 K. Doping of p-absorber p_{77}=10^{16} cm^{-3}, n^+-p junction area 20 μm × 20 μm

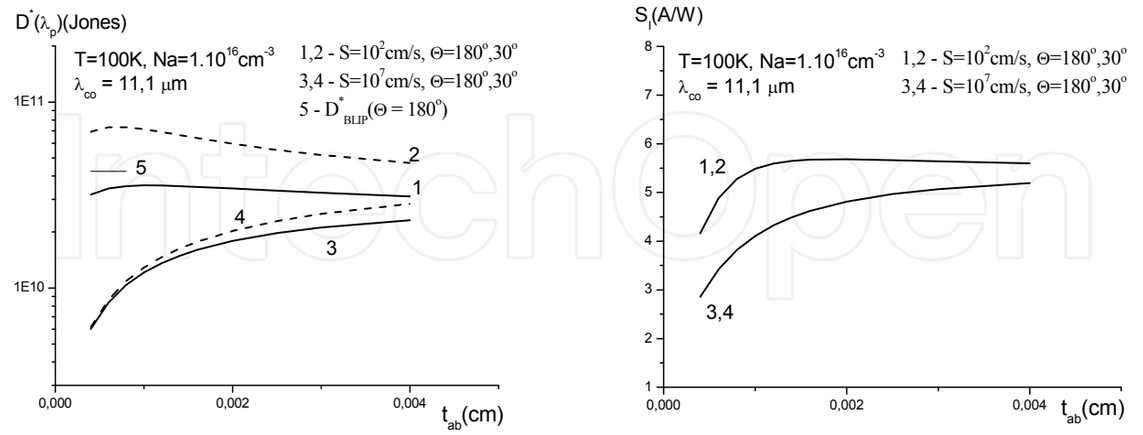

Fig. 2. Calculated peak detectivity $D^*(\lambda_p)$ and peak responsivity $S_I(\lambda_p)$ of $Hg_{0.785}Cd_{0.215}Te$ photodiodes with n^+-p junction versus thickness of p-absorber t_{ab} at FOV=180^0 – (1 and 3) and FOV=30^0 – (2 and 4). Surface recombination rate s=10^2 cm/sec (1 and 2) and s=10^7 cm/sec (3 and 4). Operating temperature 100 K. Background temperature equals to 293 K. Doping of p-absorber p_{77}=10^{16} cm^{-3}, n^+-p junction area 20 μm × 20 μm

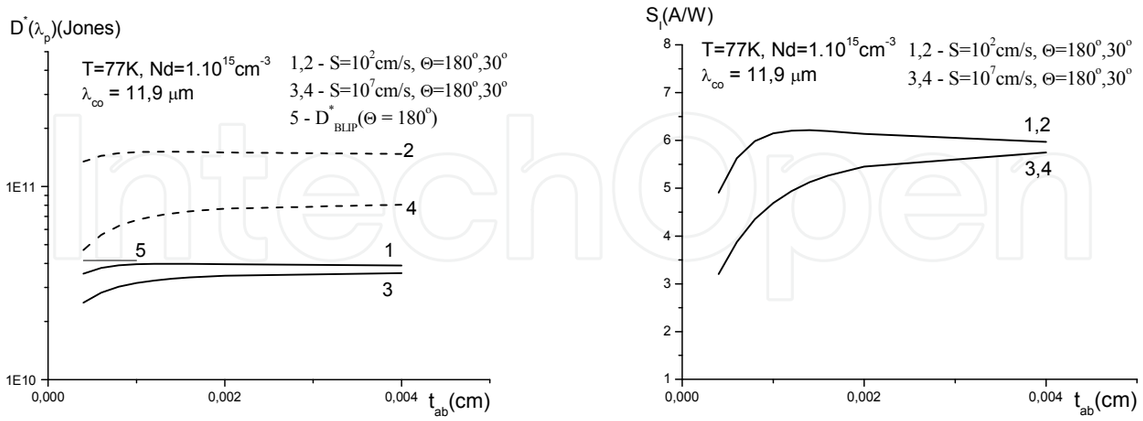

Fig. 3. Calculated peak detectivity $D^*(\lambda_p)$ and peak responsivity $S_I(\lambda_p)$ of $Hg_{0.785}Cd_{0.215}Te$ photodiodes with p-n junction versus thickness of n-absorber t_{ab} at FOV=180^0 – (1 and 3) and FOV=30^0 – (2 and 4). Surface recombination rate s=10^2 cm/sec (1 and 2) and s=10^7 cm/sec (3 and 4). Operating temperature 77 K. Background temperature equals to 293 K. Doping of n-absorber n_{77}=10^{15} cm^{-3}, p-n junction area 20 μm × 20 μm

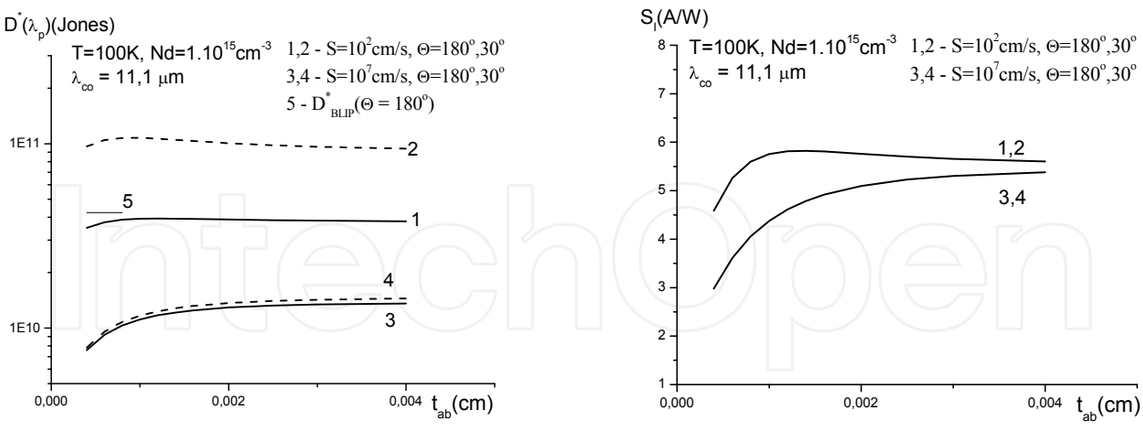

Fig. 4. Calculated peak detectivity $D^*(\lambda_p)$ and peak responsivity $S_I(\lambda_p)$ of $Hg_{0.785}Cd_{0.215}Te$ photodiodes with p-n junction versus thickness of n-absorber t_{ab} at FOV=180^0 – (1 and 3) and FOV=30^0 – (2 and 4). Surface recombination rate s=10^2 cm/sec (1 and 2) and s=10^7 cm/sec (3 and 4). Operating temperature 100 K. Background temperature equals to 293 K. Doping of n-absorber n_{77}=10^{15} cm^{-3}, p-n junction area 20 μm × 20 μm

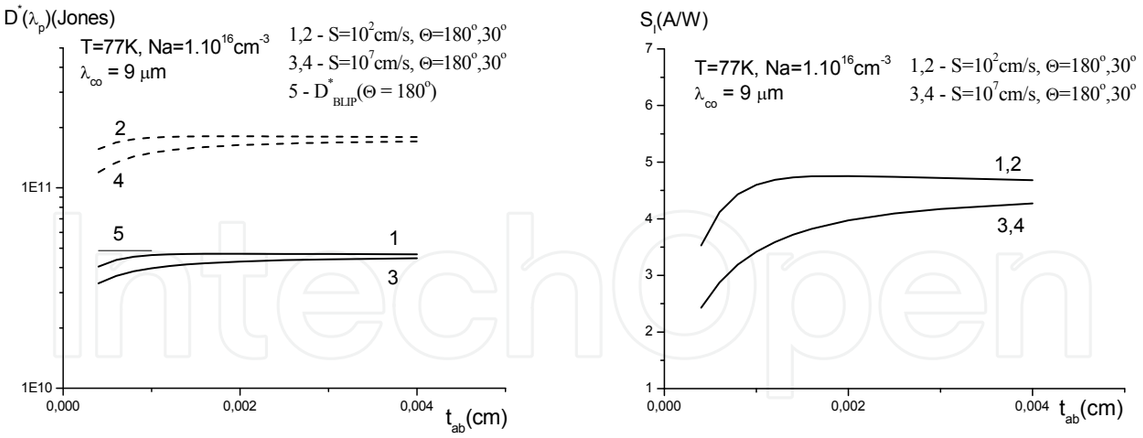

Fig. 5. Calculated peak detectivity $D^*(\lambda_p)$ and peak responsivity $S_I(\lambda_p)$ of $Hg_{0.766}Cd_{0.234}Te$ photodiodes with n^+-p junction versus thickness of p-absorber t_{ab} at FOV=180^0 – (1 and 3) and FOV=30^0 – (2 and 4). Surface recombination rate s=10^2 cm/sec (1 and 2) and s=10^7 cm/sec (3 and 4). Operating temperature 77 K. Background temperature equals to 293 K. Doping of p-absorber $p_{77}=10^{16}$ cm^{-3} , n^+-p junction area 20 μm × 20 μm

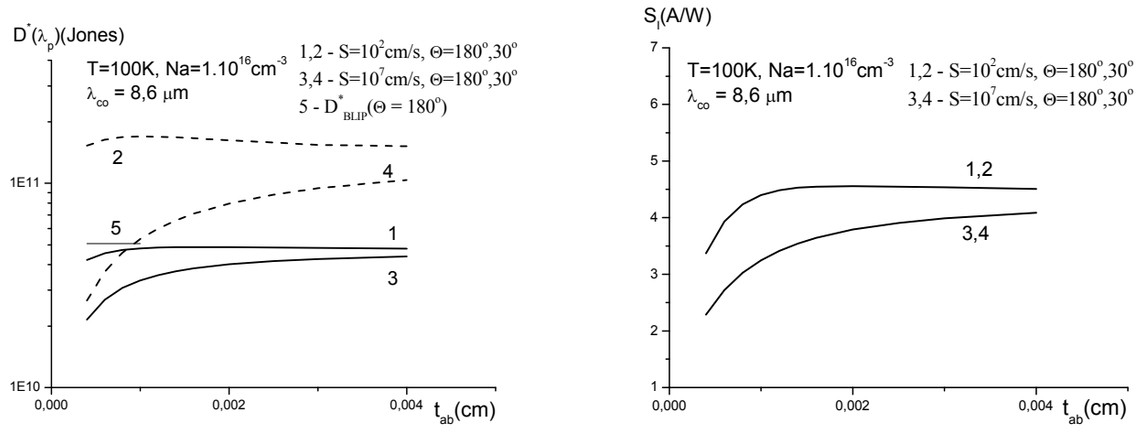

Fig. 6. Calculated peak detectivity $D^*(\lambda_p)$ and peak responsivity $S_I(\lambda_p)$ of $Hg_{0.766}Cd_{0.234}Te$ photodiodes with n^+-p junction versus thickness of p-absorber t_{ab} at FOV=180^0 – (1 and 3) and FOV=30^0 – (2 and 4). Surface recombination rate s=10^2 cm/sec (1 and 2) and s=10^7 cm/sec (3 and 4). Operating temperature 100 K. Background temperature equals to 293 K. Doping of p-absorber $p_{77}=10^{16}$ cm^{-3} , n^+-p junction area 20 μm × 20 μm

4. Surface recombination impact on currents in LWIR $Hg_{1-x}Cd_xTe$ photodiode

4.1 Approach and formalism

Cross-section of model photodiode (pixel) is shown on Fig. 7.

Dependences of dark and background currents in reverse-biased LWIR $Hg_{1-x}Cd_xTe$ photodiode on surface recombination rate S at back surface of p base ($t = LP$) were studied.

Basing on parameters of considered photodiode let's assume that:

1. Hole current inflowing into space charge region is negligible.
2. Generation-recombination current in space charge region is negligible.

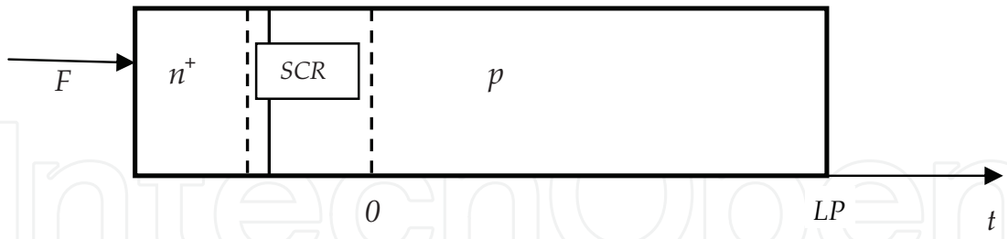

Fig. 7. Cross-section of model photodiode pixel. Here: n^+ is n^+ - region of $n^+ - p$ junction; p is base region common for all pixels of PV array. SCR is space-charge (depletion) region of $n^+ - p$ junction. Front surface of photodiode is irradiated by background photon flux F that is absorbed and generates photocurrent in photodiode. Zero point on t -axis means the boundary between space-charge region and quasi-neutral part of p base region. Point $t = LP$ is coordinate of p base region back surface

Concentration profiles of non-equilibrium dark and background generated charge carriers in p base versus t coordinate were analyzed theoretically in reversed-biased $Hg_{1-x}Cd_xTe$ photodiode at different Field-Of-View (FOV) and surface recombination rate S values. It is shown that growth of concentration of non-equilibrium dark charge carriers near SCR depends significantly on S that differs essentially from behavior of non-equilibrium background generated charge carriers. It gives in the result high growth of dark current with increasing of surface recombination rate. At the same time background current is varied low. Calculations based on obtained analytic expressions were done at temperature T = 77 K.

Continuity equation of electron current in p base of photodiode is defined by expression:

$$\frac{\partial i_n(t)}{\partial t} + q \times g(t) - q \times R_n = 0 \tag{32}$$

Where, $i_n(t)$ - electron current density, $g(t)$ – specific (per cubic centimeter) photogeneration rate of electron-hole pairs which is defined by formula:

$$g(t) = \gamma \times \eta \times F \times \exp(-\gamma \times t) \tag{33}$$

Where:

$R_n = R_p = \Delta n / \tau$ - specific band-to-band recombination rate of non-equilibrium electrons and holes; $\Delta n = n_d + n_{bgr}$ and τ - non-equilibrium electrons and holes concentrations and lifetime; n_d and n_{bgr} - concentration of non-equilibrium dark and background radiation generated charge carriers.

Dark and background generated currents flowing through photodiode were calculated at short-circuit mode of operation under low reverse-biased $V_b \le 0.05$ V.

Boundary conditions of the task are stated as follows:

$$i_n(LP) = -q \times S \times \Delta n(LP)\ ;\ \Delta n(0) = n_p \times \left\{ \exp\left[\frac{qV}{kT} \right] - 1 \right\} \tag{34}$$

Where,
S - surface recombination rate of non-equilibrium minority charge carriers (electrons) at back surface of photodiode p base (at coordinate $t = LP$; $\Delta n(0)$ - non-equilibrium charge carriers concentration at the boundary between space charge region and quasi-neutral part of p base region; n_p - concentration of equilibrium minority charge carriers (electrons) in p base and V - bias across space charge region of photodiode that is independent on illumination.
Total current I flowing through photodiode in considered conditions is formed by electrons inflowing into space charge region from quasi-neutral part of p base region:

$$I = I_n(0) = A_{pd} \times i_n(0) \tag{35}$$

Where:
A_{pd} - area of photodiode where current is formed. Please note that for the case of photodiode sensitive area and area of photodiode where current is formed are matched.
Let's assume that there is no built-in electric field in quasi-neutral parts of $n^+ - p$ junction. Solving equation (32) in diffusion approximation we find that:

$$i_n(0) = i_{bgr}(0) + i_d(0) \tag{36}$$

$$i_{bgr}(0) = q \times \eta \times Q_n = q \times \eta \times F \times \left(\frac{\gamma^2 \times L_n^2}{\gamma^2 \times L_n^2 - 1} \right) \times \left(1 - \frac{M1P}{\gamma \times L_n} \right) \tag{37}$$

$$M1P = \frac{\left(\frac{D_n}{L_n} \right) \times sh\left(\frac{LP}{L_n} \right) + S \times ch\left(\frac{LP}{L} \right) + (\gamma \times D_n - S) \times \exp(-\gamma \times LP)}{\left(\frac{D_n}{L_n} \right) \times ch\left(\frac{LP}{L_n} \right) + S \times sh\left(\frac{LP}{L_n} \right)} \tag{38}$$

$$i_d(0) = -q \times \frac{D_n}{L_n} \times \Delta n(0) \times \left[\frac{\left(\frac{D}{L_n} \right) \times sh\left(\frac{LP}{L_n} \right) + S \times ch\left(\frac{LP}{L_n} \right)}{\left(\frac{D_n}{L_n} \right) \times ch\left(\frac{LP}{L_n} \right) + S \times sh\left(\frac{LP}{L_n} \right)} \right] \tag{39}$$

Where:
$i_{bgr}(0)$ and $i_d(0)$ - background and dark components of electron current density $i_n(0)$;
D_n and L_n - electrons' diffusion coefficient and ambipolar diffusion length of charge carriers in p base defined via ambipolar diffusion coefficient of electrons in p base;
Q_n - collection coefficient of non-equilibrium photogenerated charge carriers in p base and LP - thickness of quasi-neutral part of p base region.
Concentration profiles of non-equilibrium dark $n_d(t)$ and photogenerated $n_{bgr}(t)$ charge carriers are defined by expressions (40) and (41) properly:

$$n_d(t) = \Delta n(0) \times \left[\frac{D_n \times ch\left(\frac{LP-t}{L_n}\right) + S \times L_n sh\left(\frac{LP-t}{L_n}\right)}{D_n \times ch\left(\frac{LP}{L_n}\right) + S \times L_n sh\left(\frac{LP}{L_n}\right)} \right] \quad (40)$$

$$n_{bgr}(t) = \left(\frac{\gamma \times \eta \times F \times \tau}{1 - \gamma^2 \times L_n^2} \right) \times \left[\exp(-\gamma \times t) + M2 \right] \quad (41)$$

$$M2 = \frac{(\gamma \times D_n - S) \times sh\left(\frac{t}{L_n}\right) - S \times sh\left(\frac{LP-t}{L_n}\right) - \frac{D_n}{L_n} \times ch\left(\frac{LP-t}{L_n}\right)}{S \times sh\left(\frac{LP}{L_n}\right) + \frac{D_n}{L_n} \times ch\left(\frac{LP}{L_n}\right)} \quad (42)$$

4.2 LWIR PD currents: calculation results

Data used in calculation are given in Table 2.

Data used for estimation of dark and background generated currents in small-size $Hg_{0.776}Cd_{0.224}Te$ photodiode:

	PD with n^+-p junction
Operating temperature, T	77 K
$Hg_{1-x}Cd_xTe$ absorber composition, x	0.224
Energy gap, E_g	0.12 eV
Cut-off wavelength, λ_{co}	10.3 μm
Peak wavelength, λ_p	≈ 9.2 μm
Absorption coefficient, γ	3×10^3 cm^{-1}
Quantum efficiency, η	0.7
Photodiode collection area, A_{pd}	20 μm × 20 μm = 4×10^{-6} cm^2
Thickness of quasi-neutral part of p-base, LP	10 μm=10^{-3} cm
Junction regions doping, n and p	$n^+=10^{17}$ cm^{-3}; N_A= p=5×10^{15} cm^{-3}
Bias across space charge region, V_b	-0.05 V
Minority charge carriers lifetime in p-base, τ	7.95×10^{-8} sec
Electron mobility, μ_n	1.67×10^5 $cm^2/(V\times sec)$
Hole mobility, μ_p	600 $cm^2/(V\times sec)$
Electron diffusion coefficient, D_n	1.15×10^3 cm^2/sec
Hole diffusion coefficient, D_p	4.14 cm^2/sec
Ambipolar diffusion length, L	48 μm

Table 2. Data used for estimation of dark and background generated currents in small-size $Hg_{0.776}Cd_{0.224}Te$ photodiode

Developed approach (32) - (42) was applied to calculate non-equilibrium dark and background generated concentration of minority charge carriers in *p* base and dark and background generated currents flowing through small-size $Hg_{0.776}Cd_{0.224}Te$ photodiode at low reverse bias.

Calculated dependences of non-equilibrium dark $n_d(t)$ and background generated $n_{bgr}(t)$ concentration of minority charge carriers in p base on surface recombination rate S and cold shield Field-Of-View (FOV) are shown on Fig. 8. As it is seen from Fig. 8 calculated non-equilibrium dark concentration of minority charge carriers at back boundary of p base $t = LP$ increases up to two orders in comparison with concentration at SCR boundary $t = 0$ with growing S. At the same time background generated concentration of minority charge carriers varies not so significantly in a few times only.

Respectively dark I_d and background generated I_{bgr} currents are varied with growing S analogously to variation of non-equilibrium dark and background generated concentrations of minority charge carriers (Fig. 9). To do comparison of $I_d(S)$ and $I_{bgr}(S)$ dependencies more convenient we present on Fig. 9 graphs in arbitrary units as well. Every curve is specified to its minimum. Minimum value of I_d responds S = 10^2 cm/sec and for I_{bgr} it responds S = 10^7 cm/sec. It is obvious that dark component varies in a few orders and background component near to constant.

Physical reason of that result becomes clear if we address to Fig. 8. Independently to surface recombination rate value at back surface of p base gradient of concentration of background generated minority charge carriers is practically the same near SCR (near $t = 0$). But gradient of concentration of non-equilibrium dark minority charge carriers increases rapidly with increasing S. Proper currents are proportional to gradients of proper concentrations at $t = 0$. Therefore background current is varied slightly and dark current increases significantly when surface recombination rate grows.

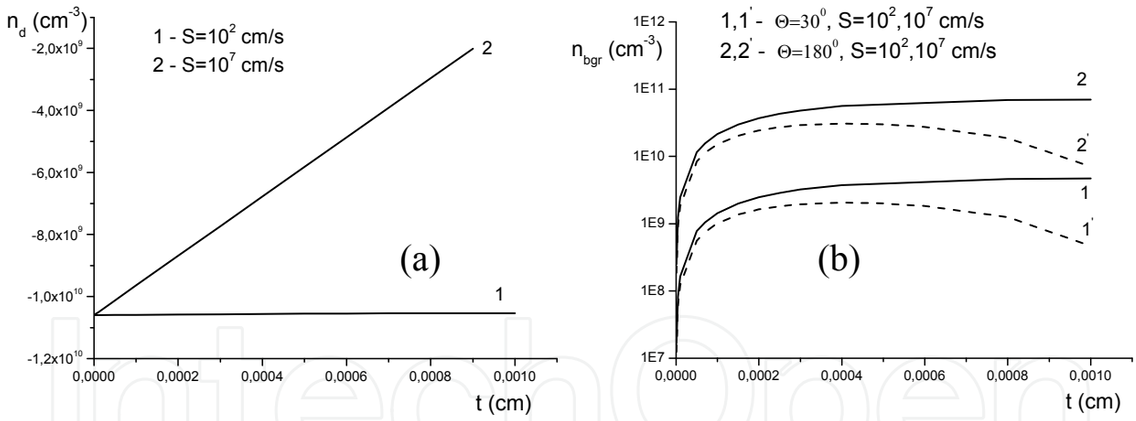

Fig. 8. Calculated concentration profiles of non-equilibrium dark $n_d(t)$ - (a) and background generated $n_{bgr}(t)$ - (b) minority charge carriers in quasi-neutral p base versus thickness t of p base at different surface recombination rate S and cold shield formed Field-Of-View (Θ) in $Hg_{1-x}Cd_xTe$ (x=0.224) photodiode described by data given in Table 2

The reason of different reaction of non-equilibrium dark and background generated charge carriers' concentration profiles on surface recombination rate's variation is as follows. In accepted conditions major share of infrared radiation is absorbed in part of p base joining to space charge region (nearby point $t = 0$). Thickness of that absorbing part is a few times smaller than total thickness LP of p base. Again thickness of p base is almost order of value less than ambipolar diffusion length $L_n \approx 10^{-2}$ cm. In addition background

concentration in zero point ($t = 0$) is always equal to zero i.e. $n_{bgr}(0)$ =0. As the result concentration profile of photogenerated charge carriers nearby to point $t = 0$ is formed preferably by their photogeneration with subsequent extraction into SCR. On the other hand due to disparity $LP << L_n$ extraction of dark minority carriers into SCR takes place from whole thickness of *p* base where they have existed initially (at V_b =0). Furthermore value of concentration $n_d(0) = \Delta n(0) < 0$ is fixed according to expression (34) by applied bias and algebraic value $n_d(LP) \le 0$ grows with increasing of S . In other words ratio $n_d(LP) / n_d(0)$ is raised. This entire means that gradient of concentration of non-equilibrium dark minority charge carriers along axis t grows with increasing of S (Fig. 8a).

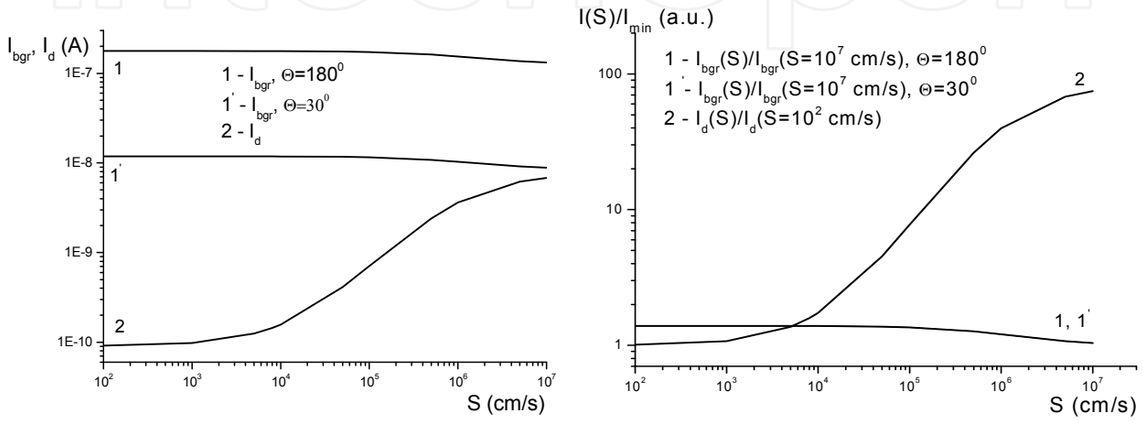

(a) (b)

Fig. 9. Dark I_d - (a) and background generated I_{bgr} - (b) currents versus S in $Hg_{1-x}Cd_xTe$ (x=0.224) photodiode described by data given in Table 2. On graph (a) currents are given in absolute units and on graph (b) – in arbitrary units when curves (a) are specified to minimum photocurrent values

5. Photocurrent generation and collection in small-pitch high-density IRFPA

Theoretical approach was developed for the case of front-side illuminated IRFPA based on regular structure of $n^+ - p$ junctions enlaced by n^+_{gr} - guard ring around, Fig. 10.

5.1 PV IRFPA design model

Cross-section of model PD array fragment (pixel) is shown on Fig. 10.

5.2 Photocurrent generated by sideways δ-shaped light beam

For estimation purpose let's consider one-dimensional (along line A) $n^+_{gr} - p - n^+_m - p - n^+_{gr}$ fragment (Fig. 10) of model PD array illuminated by δ -shaped light beam perpendicularly to surface of array, where n^+_m is n^+ - region of $n^+ - p$ junction, n^+_{gr} is n^+ - guard ring around $n^+ - p$ junction and p is layer (substrate) common for all pixels of PD array. Pixel is area including $n^+ - p$ junction and limited by guard ring (Fig. 11). Model array fragment is symmetrical regarding n^+_m - region (Fig. 11). For simplicity word photocurrent will mean further photocurrent generated by pixel illuminated by proper light. Photocurrent generated in pixel is calculated at short-circuit between lead V and Ground (Fig. 11).

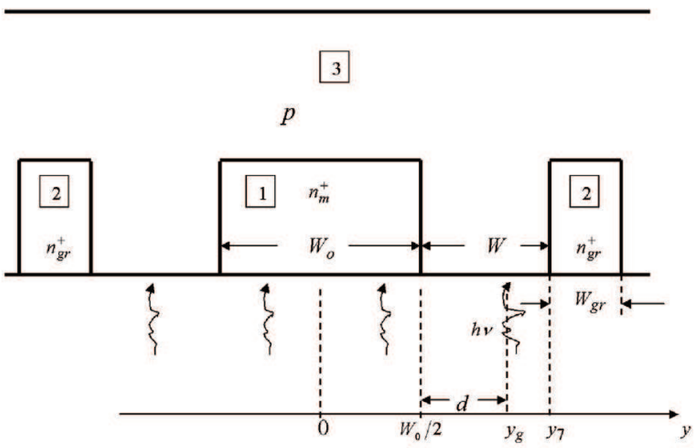

Fig. 10. Cross-section of model PD array fragment (pixel). 1 - n_m^+ is n^+ - region of $n^+ - p$ junction with width W_0 ; 2 - n_{gr}^+ is n^+ - guard ring with width W_{gr} ; 3 - p is thin layer (substrate) common for all pixels of PD array. Spacing between periphery of $n^+ - p$ junction and guard ring is marked as W . Front surface of array is irradiated by photon flux $h\nu$ (δ - shaped light beam or uniform flux or spotlight) that is absorbed and generates photocurrent

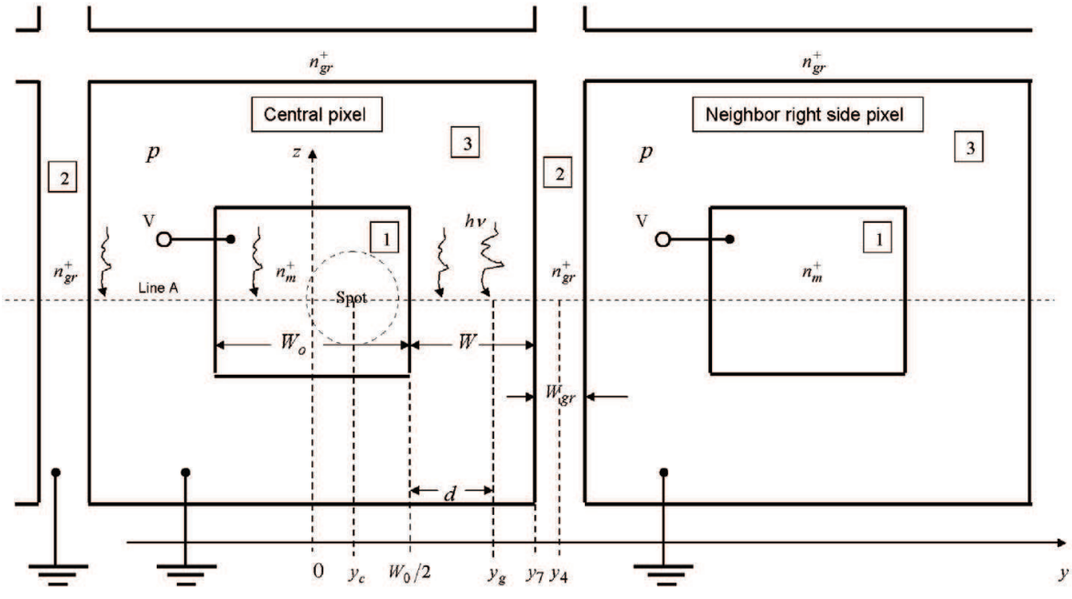

Fig. 11. Front view of model PD array fragment. 1 - n_m^+ is n^+ - region of $n^+ - p$ junction with width W_0 ; 2 - n_{gr}^+ is n^+ - guard ring with width W_{gr} ; 3 - p is thin layer (substrate) common for all pixels of PD array. Spacing between periphery of $n^+ - p$ junction and guard ring is marked as W . Front surface of array is irradiated by photon flux $h\nu$ (δ -shaped light beam or uniform flux or spotlight) that is absorbed and generates photocurrent in pixel. One-dimensional consideration is developed along line A (illumination moves along that line). Common p thin layer and n_{gr}^+ - guard ring grid are grounded. Photocurrent generated in pixel is calculated between Ground and V diode lead connected to n_m^+ - region of $n^+ - p$ junction

Let's assume:
Recombination rates of excess electrons and holes are equal to each other.

$$R_n = R_p = \frac{\Delta n}{\tau} \tag{43}$$

Where: R_n and R_p - recombination rates, Δn - concentration and τ - lifetime of excess electrons and holes.
Drift of excess charge carriers in electric field in p - region is negligible.
Band-to-band photogeneration of charge carriers at point $y = y_g$, i.e. specific rate of photogeneration is described by formula:

$$g(y) = G_\delta \times \delta(y - y_g) \tag{44}$$

Where: $\delta(y - y_g)$ - delta-function and G_δ - total photogeneration rate of charge carriers.
In analyzed conditions distribution of $\Delta n(y)$ in p - region is defined by diffusion equation:

$$D \times \frac{\partial^2 \Delta n}{\partial y^2} - \frac{\Delta n}{\tau} = -G_\delta \times \delta(y - y_g) \tag{45}$$

Where: D - coefficient of ambipolar diffusion.
Do solve equation (45) in intervals $W_o / 2 < y \le y_g$ and $y_g \le y \le y_7 \equiv W_0 / 2 + W$ assuming boundary conditions:

$$\Delta n(W_o / 2) = n_p \times \left[\exp\left(\frac{qV}{kT}\right) - 1 \right] \text{ and } \Delta n(y_7) = 0 \tag{46}$$

And stitching conditions are:

$$\Delta n(y_g - 0) = \Delta n(y_g + 0) \text{ and } D \times \left(\left.\frac{\partial \Delta n}{\partial y}\right|_{y=y_g+0} - \left.\frac{\partial \Delta n}{\partial y}\right|_{y=y_g-0} \right) = -G_\delta \tag{47}$$

Where: n_p - concentration of equilibrium minority charge carriers (electrons) in p - region.
Condition (46) means continuity of excess charge carriers' concentration, and condition (47) is derived relation resulted from integration of equation (45) in neighborhood of point $y = y_g$. Photocurrent value I_{ph}^{δ} at $y = W_0 / 2$ is defined by formula:

$$I_{ph}^{\delta} = q \times G_\delta \times K \tag{48}$$

Where: K - coefficient of one-sided sideways photoelectric conversion defined as:

$$K = \frac{sh[(W - d) / L]}{sh(W / L)}. \tag{49}$$

Where: $L = \sqrt{D \times \tau}$ - ambipolar diffusion length of charge carriers.

Graph of K versus normalized distance d/W between δ-shaped light beam and periphery of n_m^+ - region of $n^+ - p$ junction is presented on Fig. 12.
If sideways δ-shaped light beam illumination is symmetrical in relation to n^+ - region of $n^+ - p$ junction (i.e. junction is illuminated from left and right sides, Fig. 10) then total photocurrent value will be two times higher than got from expression (48).

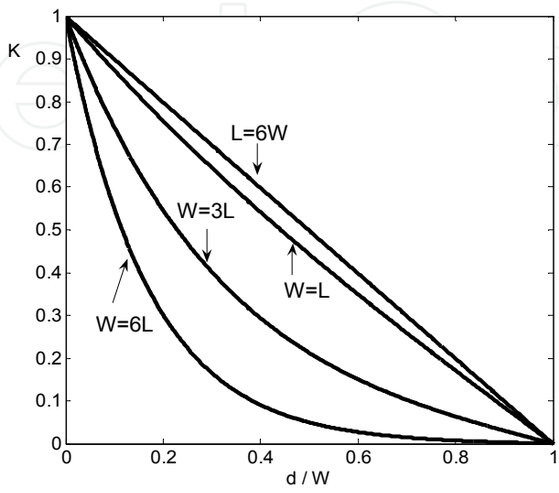

Fig. 12. Dependence of one-sided sideways photoelectric conversion coefficient K on normalized distance d/W between δ-shaped light beam and periphery of n_m^+ - region

5.3 Photocurrent generated by uniform sideways and front illumination

To calculate photocurrent value I_{ph}^{lat} under symmetrical regarding n_m^+ - region sideways illumination we need integrate expression (48) with respect to y between $W_o/2$ and W and than multiply result by coefficient 2.
In the case of uniform illumination ($G_\delta(x) = const$) we get:

$$I_{ph}^{lat} = q \times G_{2W} \times K_{tot}^{lat}. \tag{50}$$

Where: G_{2W} - total sideways photogeneration rate (taking into account both left and right sides) is defined as:

$$G_{2W} = G_\delta \times 2W \tag{51}$$

And sideways photoelectric conversion coefficient K_{tot}^{lat} if defined by:

$$K_{tot}^{lat} = \frac{L}{W} \times th\left(\frac{W}{2L}\right). \tag{52}$$

Assuming that photoelectric conversion coefficient is equal to 1 under front-side illumination we can write photocurrent value I_{ph}^{fr} in this case as follows:

$$I_{ph}^{fr} = q \times G_\delta \times W_0. \tag{53}$$

As it follows from expressions (50) - (53) ratio of photocurrents generated by $n^+ - p$ junction under uniform sideways and front-side illumination is defined by:

$$R \equiv \frac{I_{ph}^{lat}}{I_{ph}^{fr}} = 2 \times \frac{L}{W_o} \times th\left(\frac{W}{2L}\right) = 2 \times a_0 \times th\left(\frac{1}{2a}\right) = a_0 \times Y \tag{54}$$

$$a_o = L / W_o \ , \ a = L / W \text{ and } Y = 2 \times th\left(\frac{1}{2a}\right). \tag{55}$$

Graph of calculated universal dependence $Y = 2 \times th\left(\frac{1}{2a}\right)$ versus L / W is given on Fig. 13.

Herein:

$$R = a_o \times Y(L / W). \tag{56}$$

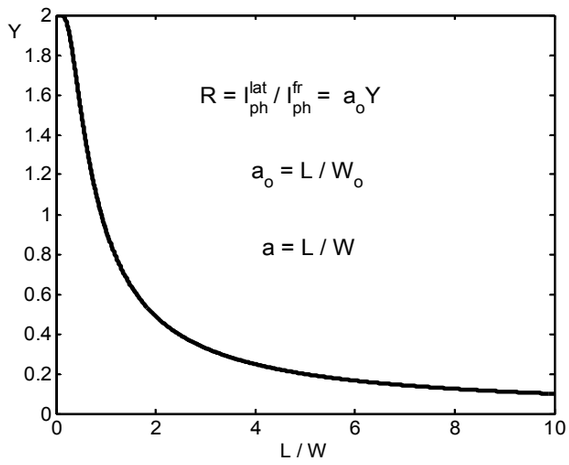

Fig. 13. Graph of universal dependence $Y = 2 \times th\left(\frac{1}{2a}\right)$ versus L / W following to (55)

5.4 Photocurrent generated by moving small-diameter uniform spotlight

Basic relation (48) allows estimating of photocurrent I_{ph} variation when small diameter (D_{spot}) uniform spotlight is moving along surface of PD array.

To calculate photocurrent value we need integrate expression (48) with respect to y within uniformly illuminated region except guard ring region (W_{gr}). Further we will limit consideration by condition (57):

$$D_{spot} \le W_o. \tag{57}$$

Within uniform spotlight area dependence of photocurrent I_{ph} on spot center position y_c will be described by formulae given further.

Case (a): Gap between n_m^+ - region border and n_{gr}^+ - guard ring is higher than spot diameter:

$$W \geq D_{spot} . \tag{58}$$

Generation of photocurrent when spot illuminates right half of central pixel.

Let's mark $I_{ph}^{(c)}$ photocurrent generated in central pixel when spot moves within interval $-W - W_0/2 \leq y \leq W_0/2 + W$.

1a. Spot center moves within the interval:

$$0 \leq y_c \leq y_1 \equiv W_0/2 - r . \tag{59}$$

In this case spot is located within n_m^+ - region of $n^+ - p$ junction totally. Photocurrent $I_{ph}^{(c)}$ is frontal only that is:

$$I_{ph}^{(c)} = I_{ph}^{fr} = q \times G_\delta \times D_{spot} . \tag{60}$$

2a. Spot center moves within the interval:

$$y_1 \leq y_c \leq y_2 \equiv W_0/2 + D_{spot}/2 . \tag{61}$$

Spot light is appearing on the side of n_m^+ - region and at $y_c > y_2$ get it away.
In the interval (61) we get:

$$\frac{I_{ph}^{(c)}(y_c)}{q \cdot G_\delta} = F_1(y_2 - y_c, y_3 - y_c) \equiv y_2 - y_c + \frac{L}{sh(W/L)} \times \left[ch\left(\frac{W}{L}\right) - ch\left(\frac{y_3 - y_c}{L}\right) \right] \tag{62}$$

$$y_3 \equiv (W_0/2) + W - D_{spot}/2 \tag{63}$$

3a. Spot center moves within the interval:

$$y_2 \leq y_c \leq y_3 . \tag{64}$$

Spotlight is located totally between n_m^+ - and n_{gr} - regions, therefore $I_{ph}^{fr} = 0$ and

$$\frac{I_{ph}^{(c)}(y_c)}{q \cdot G_\delta} = F_2(y_7 - y_c) \equiv 2L \times \frac{sh(D_{spot}/2L)}{sh(W/L)} \times sh\left(\frac{y_7 - y_c}{L}\right) . \tag{65}$$

Case (a_1): Let's impose some condition - width of guard ring is narrower than spotlight diameter:

$$W_{gr} < D_{spot} . \tag{66}$$

4a_1. Spot center moves within the interval:

$$y_3 \leq y_c \leq y_5 \equiv (W_0/2) + W + D_{spot}/2 . \tag{67}$$

Spotlight gets away gradually from considered central pixel. Photocurrents generated in central pixel and neighbor right side pixel will be equal to each other when y_c will coincide to mid y_4 of right side guard ring (68):

$$y_4 \equiv \left(W_0/2\right) + W + \left(W_{gr}/2\right). \tag{68}$$

In the interval (67):

$$\frac{I_{ph}^{(c)}(y_c)}{q \cdot G_\delta} = F_3\left(y_5 - y_c\right) \equiv 2L \times \frac{sh^2\left[\left(y_5 - y_c\right)/2L\right]}{sh\left(W/L\right)}. \tag{69}$$

5a. Spot center moves beyond coordinate y_5

$$y_c \geq y_5 . \tag{70}$$

In this case spotlight leaves central pixel entirely and no photocurrent will be generated

$$I_{ph}^{(c)}(y_c) = 0 . \tag{71}$$

Generation of photocurrent when spot illuminates left half of neighbor right side pixel.
Photocurrent generation in right side pixel $I_{ph}^{>}$ will take place when edge of spotlight appears in that pixel, i.e. at condition (72):

$$y_c \geq y_6 \equiv \left(W_0/2\right) + W + W_{gr} - D_{spot}/2 . \tag{72}$$

It means that till spot's edge hasn't reach periphery of right side pixel and no photocurrent is generated

6a. $$y_c \leq y_6 ; \;\; I_{ph}^{>}(y_c) = 0 . \tag{73}$$

Photocurrent $I_{ph}^{>}(y_c)$ and $I_{ph}^{(c)}(y_c)$ values are symmetrical about mid line of guard ring region y_4, i.e.:

$$I_{ph}^{>}(y_c) = I_{ph}^{(c)}\left(2y_4 - y_c\right). \tag{74}$$

Therefore we do have the following cases:

7a$_1$. $$y_6 \leq y_c \leq y_{11} \equiv \left(W_0/2\right) + W + W_{gr} + D_{spot}/2 ; \;\; \frac{I_{ph}^{>}}{q \times G_\delta} = F_3(y_c - y_6). \tag{75}$$

8a$_1$. $$y_{11} \leq y_c \leq y_{10} \equiv \left(W_0/2\right) + 2W + W_{gr} - D_{spot}/2 ; \;\; \frac{I_{ph}^{>}(y_c)}{q \cdot G_\delta} = F_2\left(y_c - y_9\right). \tag{76}$$

Where:

$$y_9 = \left(W_0/2\right) + W + W_{gr} . \tag{77}$$

9a$_1$. $$y_{10} \leq y_c \leq y_{12} \equiv \left(W_0/2\right) + 2W + W_{gr} + r ; \;\; \frac{I_{ph}^{>}(y_c)}{q \times G_\delta} = F_1\left(y_c - y_{10}, y_c - y_{11}\right). \tag{78}$$

10a$_1$. $$y_{12} \le y_c \le y_8 ; \ \frac{I_{ph}^{>}(y_c)}{q \times G_\delta} = D_{spot} . \tag{79}$$

Where distance between centers of n_m^+ - regions of central and right side pixels:

$$y_8 = W_0 + 2W + W_{gr} . \tag{80}$$

Generation of photocurrent when spot illuminates left half of central pixel.
Let's mark photocurrent at negative and positive coordinate y_c as $I_{ph-}(y_c)$ and $I_{ph}(y_c)$ properly. Values $I_{ph-}(y_c)$ and $I_{ph}(y_c)$ are the same in respect to zero point $y_c = 0$, i.e.

$$I_{ph-}(y_c) = I_{ph}(-y_c) . \tag{81}$$

Therefore we do have the following cases:

11a. $$-y_1 \le y_c \le 0 ; \ I_{ph-}(y_c) = q \times G_\delta \times D_{spot} . \tag{82}$$

12a. $$-y_2 \le y_c \le -y_1 ; \ I_{ph-}(y_c) = q \times G_\delta \times F_1(y_2 + y_c, y_3 + y_c) . \tag{83}$$

13a. $$-y_3 \le y_c \le -y_2 ; \ I_{ph-}(y_c) = q \times G_\delta \times F_2(y_7 + y_c) . \tag{84}$$

14a. $$-y_5 \le y_c \le -y_3 ; \ I_{ph-}(y_c) = q \times G_\delta \times F_3(y_5 + y_c) . \tag{85}$$

15a. $$y_c \le -y_5 ; \ I_{ph-}(y_c) = 0 . \tag{86}$$

Generation of photocurrent when spot illuminates right half of neighbor left side pixel.

16a. $$-y_6 \le y_c \le 0 ; \ I_{ph-}(y_c) = 0 . \tag{87}$$

17a$_1$. $$-y_{11} \le y_c \le -y_6 ; \ I_{ph-}(y_c) = q \times G_\delta \times F_3(-y_c - y_6) . \tag{88}$$

18a$_1$. $$-y_{10} \le y_c \le -y_{11} ; \ I_{ph-}(y_c) = q \times G_\delta \times F_2(-y_c - y_9) . \tag{89}$$

19a$_1$. $$-y_{12} \le y_c \le -y_{10} ; \ I_{ph-}(y_c) = q \times G_\delta \times F_1(-y_c - y_{10}, -y_c - y_{11}) . \tag{90}$$

20a$_1$. $$-y_8 \le y_c \le -y_{12} ; \ I_{ph-}(y_c) = q \times G_\delta \times D_{spot} . \tag{91}$$

Case (b): Gap between n_m^+ - region border and n^+ - guard ring is less than spot diameter:

$$W \le D_{spot} / 2 . \tag{92}$$

Generation of photocurrent when spot illuminates right half of central pixel.

21b. $$0 \le y_c \le y_1 ; \ I_{ph}^{(c)} = I_{ph}^{fr} = q \times G_\delta \times D_{spot} . \tag{93}$$

22b. $$y_1 \le y_c \le y_3\ ;\ \frac{I_{ph}^{(c)}(y_c)}{q\cdot G_\delta} = F_1\left(y_2 - y_c, y_3 - y_c\right). \tag{94}$$

In interval (96) part of spot is located in n_m^+ - region but spot edge does not reach guard ring. Case (b_1): Let's impose some condition:

b_1. $$W_{gr}/2 \le (D_{spot}/2 - W). \tag{95}$$

23b_1. $$y_3 \le y_c \le y_2\ ;\ \frac{I_{ph}^{(c)}(y_c)}{q\cdot G_\delta} = F_4\left(y_2 - y_c\right) \equiv y_2 - y_c + L\times th\left(\frac{W}{2L}\right). \tag{96}$$

24b_1. $$y_2 \le y_c \le y_5\ ;\ \frac{I_{ph}^{(c)}(y_c)}{q\cdot G_\delta} = F_3\left(y_5 - y_c\right). \tag{97}$$

25. $$y_5 \le y_c \le y_8\ ;\ I_{ph}^{(c)} = 0. \tag{98}$$

Generation of photocurrent when spot illuminates left half of neighbor right side pixel.

26. $$0 \le y_c \le y_6\ ;\ I_{ph}^{>}(y_c) = 0. \tag{99}$$

27b_1. $$y_6 \le y_c \le y_{10}\ ;\ \frac{I_{ph}^{>}(y_c)}{q\times G_\delta} = F_3\left(y_c - y_6\right). \tag{100}$$

28b_1. $$y_{10} \le y_c \le y_{11}\ ;\ \frac{I_{ph}^{>}(y_c)}{q\times G_\delta} = F_4\left(y_c - y_{10}\right). \tag{101}$$

29b_1. $$y_{11} \le y_c \le y_{12}\ ;\ \frac{I_{ph}^{>}(y_c)}{q\times G_\delta} = F_1\left(y_c - y_{10}, y_c - y_{11}\right). \tag{102}$$

30b_1. $$y_{12} \le y_c \le y_8\ ;\ \frac{I_{ph}^{>}(y_c)}{q\cdot G_\delta} = D_{spot}. \tag{103}$$

Generation of photocurrent when spot illuminates left half of central pixel.

31. $$-y_1 \le y_c \le 0\ ;\ I_{ph-}(y_c) = q\times G_\delta \times D_{spot}. \tag{104}$$

32b. $$-y_3 \le y_c \le -y_1\ ;\ I_{ph-}(y_c) = q\times G_\delta \times F_1\left(y_2 + y_c, y_3 + y_c\right). \tag{105}$$

33b_1. $$-y_2 \le y_c \le -y_3\ ;\ I_{ph-}(y_c) = q\times G_\delta \times F_4\left(y_2 + y_c\right). \tag{106}$$

34b_1. $$-y_5 \le y_c \le -y_2\ ;\ I_{ph-}(y_c) = q\times G_\delta \times F_3\left(y_5 + y_c\right). \tag{107}$$

35. $$-y_8 \le y_c \le -y_5\,;\ I_{ph-}(y_c) = 0\,. \tag{108}$$

Generation of photocurrent when spot illuminates right half of neighbor left side pixel.

36. $$-y_6 \le y_c \le 0\,;\ I_{ph-}(y_c) = 0\,. \tag{109}$$

37b$_1$. $$-y_{10} \le y_c \le -y_6\,;\ I_{ph-}(y_c) = q \times G_\delta \times F_3\left(-y_c - y_6\right). \tag{100}$$

38b$_1$. $$-y_{11} \le y_c \le -y_{10}\,;\ I_{ph-}(y_c) = q \times G_\delta \times F_4\left(-y_c - y_{10}\right). \tag{111}$$

39b$_1$. $$-y_{12} \le y_c \le -y_{11}\,;\ I_{ph-}(y_c) = q \times G_\delta \times F_1\left(-y_c - y_{10}, -y_c - y_{11}\right). \tag{112}$$

40b$_1$. $$-y_8 \le y_c \le -y_{12}\,;\ \ I_{ph-}(y_c) = q \times G_\delta \times D_{spot}\,. \tag{113}$$

5.5 LWIR PD array: calculation of photocurrent collection profiles

Data used in calculation of photocurrent generated in small-pitch high-density $Hg_{0.776}Cd_{0.224}Te$ PD array are given in Table 2. Junction regions thickness t was taken t(n^+) = 0.5 μm and t(p-absorber) = 6 μm. Surface recombination rate 10^2 cm/sec.

Developed approach (57) - (113) was applied to calculate photocurrent generated in small-pitch $Hg_{0.776}Cd_{0.224}Te$ PD array. Calculated dependences of photocurrent I_{ph} generated by spotlight in $Hg_{1-x}Cd_xTe$ (x=0.224) PD array are shown on Fig. 14 and ratio of photocurrents generated at uniform frontal and sideways illumination can be estimated easily from Fig. 14. It is seen clearly that developed approach allows analytical estimation of photocurrent generation in different close-packed PD arrays. Following to dependence presented on Fig. 13 contribution of photocurrent generated by sideways uniform illumination to total photocurrent of pixel can be too much high at not reasonable ratios between L, W and W_0. Dependences of photocurrent value I_{ph} are calculated as function of spot center position coordinate y_c for central and neighbor pixels of array. Condition $y_c = 0$ means that in start position Zero of coordinate system and spot center are matched. Length (distance) is given in units D_{spot} (spot diameter). Photocurrent is calculated in units $q \times G_\delta \times D_{spot}$. It is accepted in calculation that width of n_m^+ - region of $n^+ - p$ junction W_o = 20 μm; width of n_{gr}^+ - guard ring W_{gr} = 5 μm; spot diameter D_{spot} = 15 μm; operating temperature $T_{op} = 77K$; ambipolar diffusion length in p layer $L = 48$ μm. Spacing between periphery of $n^+ - p$ junction and guard ring W = 20 μm (a) and W = 5 μm (b). Photocurrent in central, neighbor right-side and neighbor left-side pixels are presented on graphs by solid curves, dashed curves and dash-and-dot curves properly

6. Conclusion

We have attempted to develop some general approach for simulation MWIR and LWIR PD IRFPA including estimation of major electro-optical parameters. Estimations have shown that extended LWIR $Hg_{1-x}Cd_xTe$ PD with p-n junction will be potentially of 4-5 times lower dark current value than PD with n^+-p junction at T=77 K and 2 times lower at T=100 K. Additionally extended LWIR $Hg_{1-x}Cd_xTe$ PD with p-n junction will be seriously lower

sensitive to operating temperature increasing than PD with traditional n+-p junction. We have shown that surface recombination rate value at back surface of thin *p* absorber can have serious effect on dark current in small-size LWIR $Hg_{1-x}Cd_xTe$ PD. We have developed analytical expressions describing collection of photogenerated charge carriers in small-pitch IRFPA for practical cases: uniform and small-size spotlight illumination.

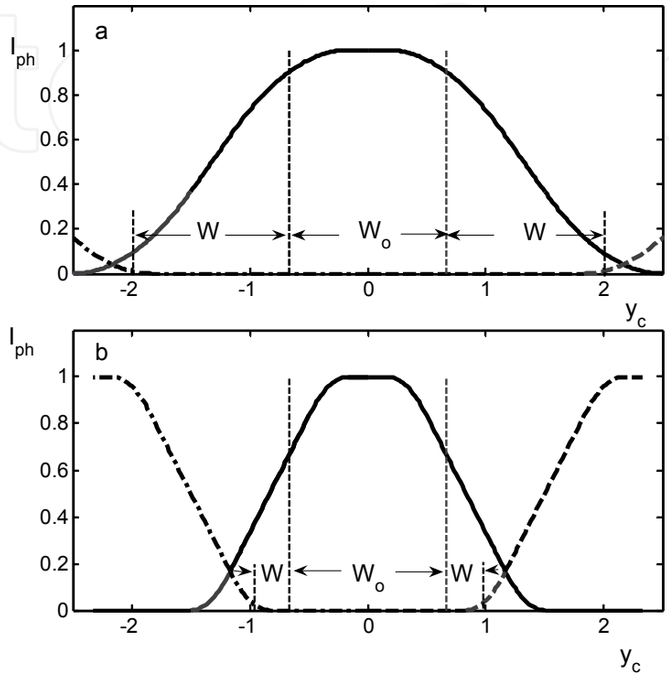

Fig. 14. Graphs of photocurrent generated in $Hg_{1-x}Cd_xTe$ (x=0.224) PD array following to expressions (57)-(113)

7. References

Whicker, S. (1992). "New technologies for FPA dewars", *Proceedings of SPIE, 1683*, pp. 102-112, ISBN 9780819408488, August 1992, SPIE Press, Bellingham, Washington

Triboulet, P. & Chatard, J.-P. (2000). "From research to production: ten years of success", *Proceedings SPIE 4130*, pp. 422-440, ISBN 9780819437754, December 2000, SPIE Press, Bellingham, Washington

Baker, I. & Maxey, C. (2001). "Summary of HgCdTe 2D array technology in the UK", *Journal of Electronic Materials*, Vol. 30, No. 6, (June 2001) 682-689, ISSN 0361-5235

Norton, P. (2002). "HgCdTe infrared detectors", *Opto-Electronics Review*, Vol. 10, No. 3, (September 2002) 159-174, ISSN 1230-3402

Kinch, M. (2007). *Fundamentals of Infrared Detector Materials*, SPIE Press, ISBN 978-0-8194-6731-7, Bellingham, Washington

Glozman, A.; Harush, E.; Jacobsohn, E.; Klin, O.; Klipstein, Ph.; Markovitz, T.; Nahum, V.; Saguy, E.; Oiknine-Schlesinger, J.; Shtrichman, I.; Yassen, M.; Yofis, B. & Weiss, E. (2006). "High performance InAlSb MWIR detectors operating at 100 K and beyond", *Proceedings SPIE 6206*, pp. 6206M, ISBN 9780819462602, May 2006, SPIE Press, Bellingham, Washington

Kinch, M.; Brau, M. & Simmons, A. (1973). "Recombination mechanisms in 8-14 μ HgCdTe", *J. Appl. Phys.*, Vol. 44, No. 4, (April 1973) 1649-1663, ISSN 0021-8979

Gelmont, B. (1980). "Auger recombination in narrow band-gap semiconductors", *Sov. Semicond. Phys. & Tech.*, Vol. 14, No. 11, (November 1980) 1913-1917, ISSN 1063-7826

Gelmont, B. (1981). "Auger recombination in narrow band-gap p-type semiconductors", *Sov. Semicond. Phys. & Tech.*, Vol. 15, No. 9, (September 1981) 1316-1319, ISSN 1063-7826

Blue, M. (1964). "Optical Absorption in HgTe and HgCdTe", *Physical Review A*, Vol. 134, No. 1, (January 1964) 226-234, ISSN 1050-2947

Laurenti, J.; Camassel, J.; Buchemadou, A.; Toulouse, B.; Legros, R. & Lusson, A., (1990). "Temperature dependence of the fundamental absorption edge of mercury cadmium telluride", *J. Appl. Phys.*, Vol. 67, No. 10, (May 1990) 6454-6460, ISSN 0021-8979

Schmit J., (1970). "Intrinsic carrier concentration of $Hg_{1-x}Cd_xTe$ as a function of x and T using k-p calculations, *J. Appl. Phys.*, Vol. 41, No. 7, (June 1970) 2876-2879, ISSN 0021-8979

Blakemore, J. (1962). *Semiconductor Statistics*, Pergamon Press, ISBN 0-486-49502-7, New York, New York

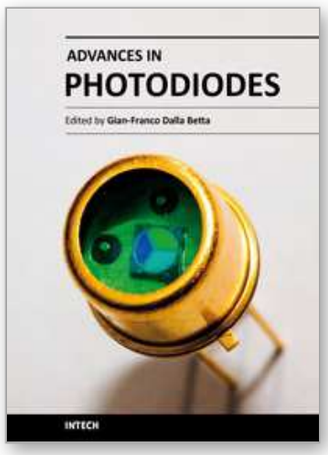

Advances in Photodiodes

Edited by Prof. Gian Franco Dalla Betta

ISBN 978-953-307-163-3
Hard cover, 466 pages
Publisher InTech
Published online 22, March, 2011
Published in print edition March, 2011

Photodiodes, the simplest but most versatile optoelectronic devices, are currently used in a variety of applications, including vision systems, optical interconnects, optical storage systems, photometry, particle physics, medical imaging, etc. Advances in Photodiodes addresses the state-of-the-art, latest developments and new trends in the field, covering theoretical aspects, design and simulation issues, processing techniques, experimental results, and applications. Written by internationally renowned experts, with contributions from universities, research institutes and industries, the book is a valuable reference tool for students, scientists, engineers, and researchers.

How to reference

In order to correctly reference this scholarly work, feel free to copy and paste the following:

Mikhail Nikitin, Albina Drugova, Viacheslav Kholodnov and Galina Chekanova (2011). Simulation of Small-pitch High-density Photovoltaic Infrared Focal Plane Arrays, Advances in Photodiodes, Prof. Gian Franco Dalla Betta (Ed.), ISBN: 978-953-307-163-3, InTech, Available from: http://www.intechopen.com/books/advances-in-photodiodes/simulation-of-small-pitch-high-density-photovoltaic-infrared-focal-plane-arrays

INTECH
open science | open minds

InTech Europe
University Campus STeP Ri
Slavka Krautzeka 83/A
51000 Rijeka, Croatia
Phone: +385 (51) 770 447
Fax: +385 (51) 686 166
www.intechopen.com

InTech China
Unit 405, Office Block, Hotel Equatorial Shanghai
No.65, Yan An Road (West), Shanghai, 200040, China
中国上海市延安西路65号上海国际贵都大饭店办公楼405单元
Phone: +86-21-62489820
Fax: +86-21-62489821

IntechOpen